Neutral-current Hall effects in disordered graphene

Yilin Wang, Xinghan Cai, Janice Reutt-Robey, and Michael S. Fuhrer

Phys. Rev. B **92**, 161411 — Published 26 October 2015

DOI: 10.1103/PhysRevB.92.161411

Neutral-current Hall effects in disordered graphene

Yilin Wang,[1,2,4] Xinghan Cai,[2] Janice Reutt-Robey[1,4] and Michael S. Fuhrer[1,2,3*]

[1]*Materials Research Science and Engineering Center, Department of Physics, University of Maryland, College Park, MD 20742, USA*

[2]*Center for Nanophysics and Advanced Materials, University of Maryland, College Park, MD 20742, USA*

[3]*School of Physics, Monash University, Victoria 3800, Australia*

[4]*Department of Chemistry and Biochemistry, University of Maryland, College Park, MD 20742, USA*

PACS numbers: 72.25.-b, 72.80.Vp, 73.63.-b, 73.20.Hb

* michael.fuhrer@monash.edu

A non-local Hall bar geometry is used to detect neutral-current Hall effects in graphene on silicon dioxide. Disorder is tuned by the addition of Au or Ir adatoms in ultra-high vacuum. A reproducible neutral-current Hall effect is found in both as-fabricated and adatom-decorated graphene. The Hall angle exhibits a complex but reproducible dependence on gate voltage and disorder, and notably breaks electron-hole symmetry. An exponential dependence on length between Hall and inverse-Hall probes indicates a neutral current relaxation length of approximately 300 nm. The short relaxation length and lack of precession in parallel magnetic field suggest that the neutral currents are valley currents. No signature of the spin-orbit coupling induced spin Hall effect is observed in the Au or Ir decorated graphene device. The near lack of temperature dependence from 7-300 K is unprecedented and promising for using controlled disorder for room temperature neutral-current electronics.

Graphene with spin degeneracy $g_s = 2$ and valley degeneracy $g_v = 2$ allows charge-neutral currents of spin or valley polarization, the subject of intense theoretical and experimental interest [1-11]. Their experimental manifestation is a neutral (spin, valley) Hall effect in which a charge current j drives a transverse neutral current j_n of either spin (j_s) or valley (j_v) polarization. Graphene is not expected to spontaneously break inversion or time-reversal symmetries, and has very weak spin-orbit coupling [12-14]. Hence the interaction between charge and spin/valley currents in perfect graphene is negligible. However, various schemes have realized strong coupling between charge and neutral currents in graphene. Neutral currents in graphene with sp^3 chemical bonding [6, 7] were interpreted as a spin Hall effect (SHE) due to enhanced spin-orbit coupling, though a recent report rejects that interpretation [11]. Inversion symmetry breaking through interaction with a substrate [8] or via perpendicular electric field in bilayer graphene [9, 10] can induce a valley Hall effect (VHE). However as-fabricated graphene devices have not been expected to exhibit neutral Hall effects.

Here we search for neutral Hall effects in graphene on silicon dioxide as-fabricated and after deposition of 5*d* electron-containing Au and Ir. Ir adatoms have been predicted to add strong spin-orbit coupling in graphene [15], and Au adatoms have been experimentally implicated in neutral Hall currents attributed to spin-orbit coupling [16]. We use the non-local Hall bar geometry [3, 5, 7, 8, 16] in which a non-local resistance signal R_{NL} is generated through neutral Hall and neutral inverse Hall effects. Surprisingly, we observe a clear and reproducible neutral Hall effect in as-fabricated graphene. On deposition of Au and Ir we observe a reduction of the charge carrier mobility consistent with a small charge transfer from Au/Ir to graphene. The neutral Hall angle $\gamma_n = j_n/j$ exhibits a complex but reproducible dependence on gate voltage and disorder, and notably breaks electron-hole symmetry. An exponential dependence on length between Hall and inverse-Hall probes indicates a neutral

current relaxation length of approximately 300 nm. We observe no sign of a spin-orbit gap opening in graphene down to a temperature of 7 K, and a negligible dependence of R_{NL} on parallel magnetic field, inconsistent with the precession expected for spin currents. The observations rule out spin as the neutral current type, and also indicate that Au and Ir adatoms do not significantly enhance the spin-orbit coupling in graphene. We conclude that that the neutral Hall effect in both as-fabricated and adatom-decorated graphene is a disorder-induced VHE. The near lack of temperature dependence from 7-300 K is unprecedented for VHE in graphene [8-10] and promising for room temperature valleytronic devices.

Figure 1(a) shows a typical atomic force microscopy (AFM) image of our Hall bar geometry. A charge current, I_{NL}, injected across one cross of the Hall bar, generates a nonlocal voltage, V_{NL}, transverse to another cross of the Hall bar. The nonlocal resistance is $R_{NL} = V_{NL}/I_{NL}$. The (local) longitudinal resistivity ρ_{xx} is measured as usual. Graphene flakes are obtained by mechanical exfoliation of graphite on a 300-nm-SiO_2/Si substrate and two electron beam lithography steps establish Cr/Au (5 nm/100 nm) electrodes and define the Hall bar via oxygen plasma etching. After annealing in H_2/Ar gas at 350 ºC to remove resist residue [17], the device was mounted on a cryostat in an ultra-high vacuum (UHV) chamber. The widths w for all devices are 0.9 um and the lengths L between two Hall bar junctions ranged from 1.8 to 3.2 um. All measurements were taken by lock-in techniques at a low frequency of 3.7 Hz. A high input impedance (1 TΩ at dc) voltage preamplifier was used to eliminate artifacts in the nonlocal measurement [9].

Adatoms (Au, Ir) were deposited via electron-beam evaporator in UHV. To vary the coverage, the device was exposed to a controlled flux in sequential time intervals at sample temperature of 7 K. Figure 1(b) shows the gate-voltage dependence of the local conductivity $\sigma_{xx}(V_g) = [\rho_{xx}(V_g)]^{-1}$ for pristine and Au-decorated graphene with $L/w = 2.9$. For pristine graphene, the gate voltage of minimum conductivity $V_{g,\,min}$ is located at 45 V and the mobility

μ is only ~ 5000 cm^2/Vs, indicating the as-fabricated device is strongly *p*-type doped and rather disordered. Upon cooling from 300 K to 7 K, the overall shape of $\sigma_{xx}(V_g)$ is the same with a slight increase in mobility. Adatom doping gradually shifts the $V_{g,\,min}$ to more negative gate voltage (*n*-type doping), lowers the mobility to ~ 1000 cm^2/Vs and decreases the minimum conductivity σ_{min}. Figure 1(c) shows the shift of $V_{g,\,min}$ as a function of Au coverage. At low doping level, the shift in $V_{g,\,min}$ is roughly linear in coverage, with an estimated charge transfer of ~0.005 *e* per adatom, while at higher coverages, the shift of $V_{g,\,\mathrm{min}}$ is sublinear in coverage. As the coverage is on order 1 ML the Au is likely clustered [18, 19], with each cluster transferring on order one charge. Then the sublinearity reflects a growth in cluster size. The reduction of mobility with shift in $V_{g,\,min}$ [Fig. 1(c) inset] is quantitatively similar to that of the previous work using potassium adatoms on graphene [20], indicating the Au clusters act as charged impurities.

We also studied the temperature dependence of ρ_{xx} of graphene with Au and Ir adatoms to search for an energy gap induced by spin orbit coupling [15] or inversion symmetry breaking [8]. Figure 1(d) shows $\rho_{xx}(T)$ for graphene with Au adatom decoration. $\rho_{xx}(T)$ is very weakly insulating, rising slightly faster than logarithmically with decreasing temperature. $\rho_{xx}(T)$ is poorly described by a simple thermal activation model $\rho_{xx} \propto e^{E_g/k_BT}$; i.e. no activated behavior is seen [21, 22], and we conclude any gap is much smaller than the disorder scale set by electron-hole puddling, on order 50 meV.

Figure 2(a) presents the gate-voltage dependence of R_{NL} for pristine and Au-decorated graphene device with L/w = 2.9. A peak in $R_{NL}(V_g)$ is evident for both pristine and Au-decorated graphene and shifts toward negative V_g after doping, which is consistent with the shift of $V_{g,\,min}$. However, the peak magnitude does not increase with increasing Au coverage, although the local resistance ρ_{xx} increases significantly. The width of the $R_{NL}(V_g)$ peak

becomes broader after doping. $R_{NL}(V_g)$ for pristine graphene shows little temperature dependence, having almost the same amplitude in 300 K and 7 K [Fig. 2(a)] and is also much greater than the expected Ohmic contribution to the non-local resistance $R_{NL,Ohmic} = \rho_{xx} e^{-\pi L/w}$ (~1 Ω). We also verified that V_{NL} is linear in I_{NL}, ruling out a thermoelectric source [5] of R_{NL}[21]. Figure 2(b) shows the ratio of R_{NL}/ρ_{xx} as a function of shifted gate voltage (V_g - $V_{g,min}$) for pristine and Au-decorated graphene. R_{NL}/ρ_{xx} is not constant (as would be expected for the Ohmic contribution) but rather strongly peaked near $V_{g,min}$ as observed previously for neutral Hall currents in graphene [7, 8]. However, in this case R_{NL}/ρ_{xx} exhibits a noticeable electron-hole asymmetry not previously observed. We find that the asymmetric peak can be well fit by a Breit-Wigner-Fano (BWF) resonance function: $\frac{R_{NL}}{\rho_{xx}} = A_0 + A_1 \frac{\left[q + \tilde{V}_g\right]^2}{1 + \tilde{V}_g^{\,2}}$, where A_1 is the amplitude of the resonance, q is the asymmetry parameter, where we define a dimensionless gate voltage $\tilde{V}_g \equiv \frac{V_g - V_{g,\min} - V_{g,res}}{\Gamma}$, where Γ is the width. A Fano resonance indicates two contributions, traditionally the interference between discrete and continuum states. In disordered graphene, a Fano resonance may arise naturally in phenomena involving a localized impurity state (discrete state) and the Dirac bands (continuum). The BWF line shape has been found in graphene in various kinds of phenomena [23-27] to reveal the electron-hole excitations in the vicinity of the Dirac cone.

Figure 3 shows the BWF fitting parameters for pristine and Au-decorated graphene at various L/w ratios. (The gate-voltage dependence of R_{NL} and R_{NL}/ρ_{xx} for pristine and Au-decorated graphene with other L/w ratios are shown in [21]). Figures 3 (a-c) show the fitting parameters A_1, q and Γas a function of mobility. The amplitude A_1 is roughly independent of mobility [Fig. 3(a)] while the asymmetry parameter q is roughly proportional to mobility [Fig.

3(b)]. The width of the BWF peak Γ decreases with increasing mobility, and the magnitude is roughly consistent with the dependence of the width of the minimum conductivity region on mobility as observed for charged impurity disorder [20, 28]. Figure 3(d) shows A_1 depends exponentially on length with similar magnitude and decay length for several L/w electrode pairs on three pristine graphene devices. We conclude that there is no qualitative difference in behavior between pristine and Au-decorated graphene. For Ir-decorated graphene devices, we observed very similar features [21, 22]: Ir adatoms also act as charged impurities and donate electrons to graphene (~0.01 e per atom). The ratio of R_{NL}/ρ_{xx} as a function of $V_g - V_{g,min}$ is also well fit by BWF resonance function, with similar trend of the fitting parameters with disorder and aspect ratio.

For a neutral Hall effect it can be shown that [7, 8]:

$$\frac{R_{NL}}{\rho_{xx}} = \frac{1}{2}(w/\xi)e^{-L/\xi}\gamma_n^2 \qquad (1)$$

where γ_n is the neutral Hall angle and ξ is the scattering length. By fitting the data in Fig. 3(d) to Eq. (1), we find ξ is consistently in the range of 250-400 nm. This ξ value is consistent with the measured intervalley scattering length in exfoliated graphene flakes on SiO_2 [29] and is much shorter than the measured spin scattering lengths of 3 - 12 um for graphene [30] [note that the data in Fig. 3(d) correspond to as-fabricated devices with no adatoms]. We have also measured the parallel magnetic field dependence $B_{||}$ of R_{NL} for as-fabricated graphene, as shown in Fig. 4. We find a small negative MR of less than 10%, consistent with a small weak localization effect due to parallel field penetrating the corrugations of graphene on SiO_2 [31]. If γ_n represented a SHE then spin precession in parallel magnetic field (the Hanle effect [32]) would cause $R_{NL}(B_{||})$ to oscillate and reverse sign (see Supplemental Material Fig. S6 [21]). Assuming that R_{NL} originates from SHE and

the spin scattering length $\lambda_s = \xi$=300 nm, we find the spin relaxation time τ_s=1.2 ps. The red curves in Fig. 4 show the corresponding expected $R_{NL}(B_{||})$ due to Hanle spin precession. We also show $R_{NL}(B_{||})$ for a hypothetical device with λ_s = 3000 nm and τ_s=100 ps (comparable to that measured by other groups [30]). No evidence of precession up to a field of 6 T is seen. The lack of precession indicates that the neutral current is not a spin current induced by SHE. Taken together, these features indicate that the observed neutral Hall effect is due to VHE, not SHE; $\gamma_n = \gamma_v$.

Comparing the BWF formula to Eq. (1), we find $\gamma_v^2 \propto \frac{\left[q + \tilde{V}_g\right]^2}{1+\tilde{V}_g^{\,2}}$. This suggests two contributions to γ_v : One contribution has $\left|\gamma_{v,1}\right| \propto \frac{\left|\tilde{V}_g\right|}{\sqrt{1+\tilde{V}_g^{\,2}}}$ and the other has $\left|\gamma_{v,2}\right| \propto \frac{q}{\sqrt{1+\tilde{V}_g^{\,2}}} \propto \frac{\mu}{\sqrt{1+\tilde{V}_g^{\,2}}}$. The fact that the contributions are added and then squared, indicates that they result from the same type of neutral current, which must be valley. The VHE requires inversion symmetry breaking. We hypothesize that disorder breaks inversion symmetry locally, leading to a VHE. While a microscopic theory of disorder induced VHE is lacking, we compare to the results for graphene with spin-orbit coupling. Sinitsyn *et al* [33] studied graphene with a spin-orbit gap, and found for correlated disorder a constant Hall angle independent of the disorder potential strength and of the concentration of scatters. Resonant scatters (skew scattering) in graphene with spin-orbit coupling tend to give Hall angles that are inversely proportional to the impurity concentration, large for Fermi energies near the resonance energy, and antisymmetric in Fermi energy about the resonance. This suggests that $\gamma_{v,1}$ (with magnitude roughly independent of V_g) results from correlated charge disorder, is an even function of $\tilde{V}_g$, and dominates in the highly charge-disordered sample,

while $\gamma_{v,2}$ (with magnitude increasing with decreasing V_g) results from resonant scattering from mid-gap states induced by skew scatters, is an odd function of $\widetilde{V}_g$, and is most important in relatively clean samples.

One important question is: What determines the overall sign of $\gamma_{v,1}$ and $\gamma_{v,2}$? The experimental setup probes only γ_v^2 since the injection and detection of the valley current are accomplished through the same mechanism, and each is proportional to γ_v . However opposite signs of γ_v in the injector and detector would produce an overall negative R_{NL}, which is never observed in 16 injector/detector pairs on 4 samples. Disorder induced by atomically sharp defects, such as structural defects, chemisorbed species, and substitutional defects, breaks the hexagonal symmetry of the honeycomb lattice and results in intervalley scattering [34, 35]. We have indirect evidence that the disorder may be important: We found a device with very small $V_{g,\,min}$ near 0 ($|V_{g,\,min}|< 0.5$ V) and mobility >10000 cm^2/Vs; the $\sigma_{xx}(V_g)$ is shown in Supplemental Material Fig. S7(a) [21]. In contrast to the previous devices with $V_{g,\,min} > 40$ V, this device exhibited no measurable gate dependent R_{NL}[21] for a L/w ratio of 3.2.

As shown in Fig. 2(a), R_{NL} has near the same amplitude and shape at both 300 K and 7 K. The lack of temperature dependence reflects the energy scale of disorder induced VHE is very large. The energy difference between the A and B sublattices for a point defect such as a vacancy is locally on order the bandwidth, ~7.5 eV [36]. For a Coulomb impurity situated 3 Å above atom A, the energy difference between the A and B sublattices is ~0.5 eV. In both cases the energy scales are much greater than room temperature, which, if the disorder may be understood and controlled, provides an effective path to room temperature valleytronics in graphene.

Lastly, we note that a very recent experimental study of R_{NL} in hydrogenated graphene [11] found a similar decay length ξ and lack of temperature and magnetic field dependence as seen here. This work casts doubt on the previous interpretation of R_{NL} in hydrogenated graphene as due to SHE [6, 7], and opens the possibility of a disorder-induced VHE in that system as well.

References

[1] A. Rycerz, J. Tworzydlo, and C. W. J. Beenakker, Nat. Phys. **3**, 172 (2007).

[2] D. Xiao, W. Yao, and Q. Niu, Phys. Rev. Lett. **99**, 236809 (2007).

[3] D. A. Abanin, S. V. Morozov, L. A. Ponomarenko, R. V. Gorbachev, A. S. Mayorov, M. I. Katsnelson, K. Watanabe, T. Taniguchi, K. S. Novoselov, L. S. Levitov, and A. K. Geim, Science **332**, 328 (2011).

[4] D. A. Abanin, R. V. Gorbachev, K. S. Novoselov, A. K. Geim, and L. S. Levitov, Phys. Rev. Lett. **107**, 096601 (2011).

[5] J. Renard, M. Studer, and J. A. Folk, Phys. Rev. Lett. **112**, 116601 (2014).

[6] A. H. Castro Neto and F. Guinea, Phys. Rev. Lett. **103**, 026804 (2009).

[7] J. Balakrishnan, G. Kok Wai Koon, M. Jaiswal, A. H. Castro Neto, and B. Özyilmaz, Nat. Phys. **9**, 284 (2013).

[8] R. V. Gorbachev, J. C. W. Song, G. L. Yu, A. V. Kretinin, F. Withers, Y. Cao, A. Mishchenko, I. V. Grigorieva, K. S. Novoselov, L. S. Levitov, and A. K. Geim, Science **346**, 448 (2014).

[9] M. Sui, G. Chen, L. Ma, W. Shan, D. Tian, K. Watanabe, T. Taniguchi, X. Jin, W. Yao, D. Xiao, and Y. Zhang, arXiv:1501.04685.

[10] Y. Shimazaki, M. Yamamoto, I. V. Borzenets, K. Watanabe, T. Taniguchi, and S. Tarucha, arXiv:1501.04776.

[11] A. A. Kaverzin and B. J. van Wees, Phys. Rev. B **91**, 165412 (2015).

[12] D. Huertas-Hernando, F. Guinea, and A. Brataas, Phys. Rev. B **74**, 155426 (2006).

[13] H. Min, J. E. Hill, N. A. Sinitsyn, B. R. Sahu, L. Kleinman, and A. H. MacDonald, Phys. Rev. B **74**, 165310 (2006).

[14] Y. Yao, F. Ye, X.-L. Qi, S.-C. Zhang, and Z. Fang, Phys. Rev. B **75**, 041401 (2007).

[15] J. Hu, J. Alicea, R. Wu, and M. Franz, Phys. Rev. Lett. **109**, 266801 (2012).

[16] J. Balakrishnan, G. K. W. Koon, A. Avsar, Y. Ho, J. H. Lee, M. Jaiswal, S.-J. Baeck, J.-H. Ahn, A. Ferreira, M. A. Cazalilla, A. H. C. Neto, and B. Özyilmaz, Nat Commun **5**, 4748 (2014).

[17] M. Ishigami, J. H. Chen, W. G. Cullen, M. S. Fuhrer, and E. D. Williams, Nano Lett. **7**, 1643 (2007).

[18] K. M. McCreary, K. Pi, A. G. Swartz, W. Han, W. Bao, C. N. Lau, F. Guinea, M. I. Katsnelson, and R. K. Kawakami, Phys. Rev. B **81**, 115453 (2010).

[19] Y. Wu, W. Jiang, Y. Ren, W. Cai, W. H. Lee, H. Li, R. D. Piner, C. W. Pope, Y. Hao, H. Ji, J. Kang, and R. S. Ruoff, Small **8**, 3129 (2012).

[20] J. H. Chen, C. Jang, S. Adam, M. S. Fuhrer, E. D. Williams, and M. Ishigami, Nat. Phys. **4**, 377 (2008).

[21] See Supplemental Material for additional data.

[22] Yilin Wang, S. Xiao, X. Cai, W. Bao, J. Reutt-Robey, and M. S. Fuhrer, arXiv: 1507.02773.

[23] K. F. Mak, J. Shan, and T. F. Heinz, Phys. Rev. Lett. **106**, 046401 (2011).

[24] E. H. Hasdeo, A. R. T. Nugraha, M. S. Dresselhaus, and R. Saito, Phys. Rev. B **90**, 245140 (2014).

[25] T.-T. Tang, Y. Zhang, C.-H. Park, B. Geng, C. Girit, Z. Hao, M. C. Martin, A. Zettl, M. F. Crommie, S. G. Louie, Y. R. Shen, and F. Wang, Nat Nano **5**, 32 (2010).

[26] D.-H. Chae, T. Utikal, S. Weisenburger, H. Giessen, K. v. Klitzing, M. Lippitz, and J. Smet, Nano Lett. **11**, 1379 (2011).

[27] D. Yoon, D. Jeong, H.-J. Lee, R. Saito, Y.-W. Son, H. C. Lee, and H. Cheong, Carbon **61**, 373 (2013).

[28] S. Adam, E. H. Hwang, V. M. Galitski, and S. Das Sarma, Proc. Natl. Acad. Sci. U.S.A. **104**, 18392 (2007).

[29] F. V. Tikhonenko, D. W. Horsell, R. V. Gorbachev, and A. K. Savchenko, Phys. Rev. Lett. **100**, 056802 (2008).

[30] W. Han, R. K. Kawakami, M. Gmitra, and J. Fabian, Nat Nano **9**, 794 (2014).

[31] M. B. Lundeberg and J. A. Folk, Phys. Rev. Lett. **105**, 146804 (2010).

[32] M. Johnson and R. H. Silsbee, Phys. Rev. B **37**, 5312 (1988).

[33] N. Sinitsyn, J. Hill, H. Min, J. Sinova, and A. MacDonald, Phys. Rev. Lett. **97**, 106804 (2006).

[34] V. V. Cheianov and V. I. Fal'ko, Phys. Rev. Lett. **97**, 226801 (2006).

[35] E. McCann, K. Kechedzhi, V. I. Fal'ko, H. Suzuura, T. Ando, and B. L. Altshuler, Phys. Rev. Lett. **97**, 146805 (2006).

[36] F. Banhart, J. Kotakoski, and A. V. Krasheninnikov, ACS Nano **5**, 26 (2010).

Figure Captions :

FIG. 1. (Color online) (a) AFM image of our graphene device. The width w and length L of the Hall bar, and the configuration of current I_{NL} and voltage probes V_{NL} for measurement of the non-local resistance are indicated. (b) The conductivity σ_{xx} versus gate voltage V_g for L/w = 2.9 for as-fabricated graphene and at three different Au coverages. Here 1 ML = 1.4 x 10^{15} cm^{-2} for Au(111). (c) The shift of gate voltage of minimum conductivity $-\Delta V_{g,min}$ as a function of Au coverage. The inset shows the $-\Delta V_{g,min}$ *vs*. inverse mobility; here all $-\Delta V_{g,min}$ values are offset by 10 V to account for initial disorder. Lines correspond to the theory in Ref. 20. (d) Temperature dependence of ρ_{xx} at $V_g = V_{g,min}$ for Au-decorated graphene.

FIG. 2. (Color online) (a) Non-local resistance R_{NL} versus V_g curves for as-fabricated and Au-decorated graphene with L/w = 2.9. The dashed and solid black curves correspond to as-fabricated graphene at 300 K and 7 K, respectively. (b) The ratio of $\frac{R_{NL}}{\rho_{xx}}$ as a function of shifted gate voltage $V_g - V_{g,min}$ for as-fabricated and Au-decorated graphene with L/w = 2.9. The solid lines are a fit to a Breit-Wigner-Fano function as described in text.

FIG. 3. (Color online) (a) - (c) The parameters of the Breit-Wigner-Fano function A_1 (a), q (b) and Γ(c) as a function of mobility at various L/w ratios. Parameters are described in text. (d) The fitting parameter A_1 for three different as-fabricated graphene devices as a function of length.

FIG. 4. (Color online) R_{NL} for as fabricated graphene device with L = 1.4 um and w = 0.9 um at $V_g - V_{g,min}$ = 5 V as a function of parallel magnetic field $B_{||}$. The squares and black line are the measured data, the dotted black line is the calculated Ohmic contribution and the red lines

are calculated Hanle precession for λ_s = 300 nm, τ_s =1.2 ps (solid red line) and λ_s = 3000 nm, τ_s =100 ps (dashed red line).

Figure 1.

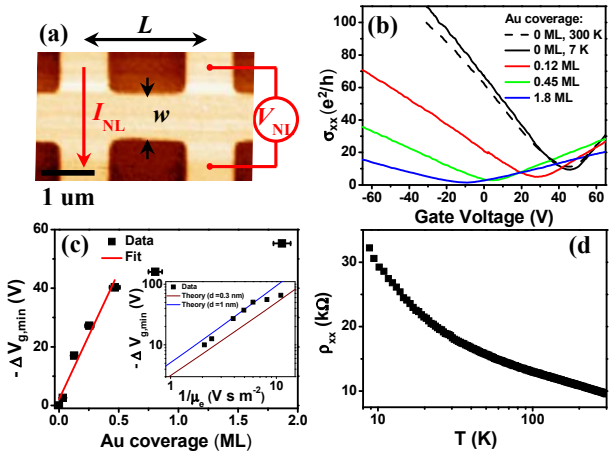
(a)
L
I_NL
w
V_NL
1 um
(b)
Au coverage:
0 ML, 300 K
0 ML, 7 K
0.12 ML
0.45 ML
1.8 ML
σxx (e²/h)
Gate Voltage (V)
(c)
Data
Fit
- ΔVg,min (V)
Au coverage (ML)
Theory (d =0.3 nm)
Theory (d =1 nm)
1/μe (V s m⁻²)
(d
ρxx (KΩ)
T (K)

Figure 2.

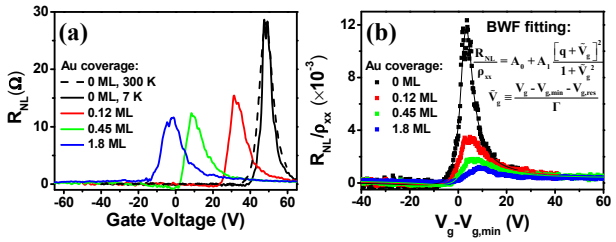
(a)
Au coverage:
0 ML, 300 K
0 ML, 7 K
0.12 ML
0.45 ML
1.8 ML
R_NL (Ω)
Gate Voltage (V)
(b)
BWF fitting:
Au coverage:
0 ML
0.12 ML
0.45 ML
1.8 ML
R_NL/ρ_xx (×10^-3)
V_g-V_g,min (V)

Figure 3.

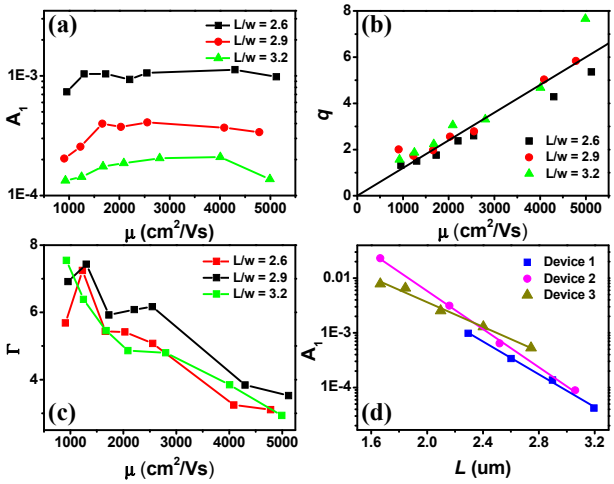
(a)
L/w = 2.6
L/w = 2.9
L/w = 3.2
A1
1E-3
1E-4
1000 2000 3000 4000 5000
μ (cm2/Vs)
(b)
q
0 2 4 6 8
0 1000 2000 3000 4000 5000
μ (cm2/Vs)
(c)
Γ
4 6 8
1000 2000 3000 4000 5000
μ (cm2/Vs)
(d)
Device 1
Device 2
Device 3
A1
0.01
1E-3
1E-4
1.6 2.0 2.4 2.8 3.2
L (um)

Figure 4.

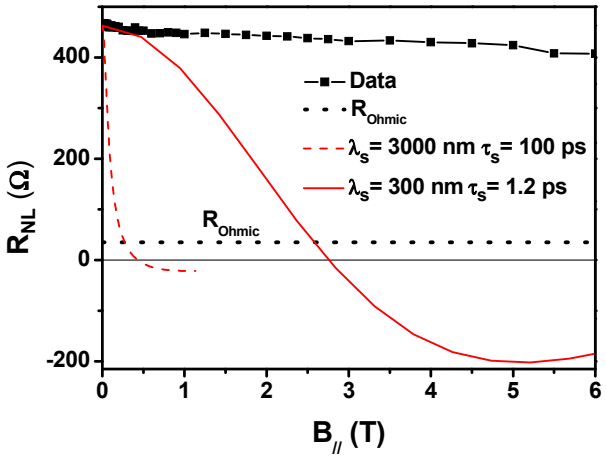
400
200
0
-200
0
1
2
3
4
5
6
R_{NL} (Ω)
$B_{//}$ (T)
Data
R_{Ohmic}
λ_s= 3000 nm τ_s= 100 ps
λ_s= 300 nm τ_s= 1.2 ps
R_{Ohmic}